

Towards a Resource-Optimized Dynamic Quantum Algorithm via Non-iterative Auxiliary Subspace Corrections

Chayan Patra,¹ Debaarjun Mukherjee,¹ Sonaldeep Halder,¹ Dibyendu Mondal,¹ and Rahul Maitra^{1,2, a)}

¹⁾*Department of Chemistry,
Indian Institute of Technology Bombay,
Powai, Mumbai 400076, India*

²⁾*Centre of Excellence in Quantum Information, Computing, Science & Technology,
Indian Institute of Technology Bombay,
Powai, Mumbai 400076, India*

Recent quantum algorithms pertaining to electronic structure theory primarily focus on threshold-based dynamic construction of ansatz by selectively including important many-body operators. These methods can be made systematically more accurate by tuning the threshold to include more number of operators into the ansatz. However, such improvements come at the cost of rapid proliferation of the circuit depth, especially for highly correlated molecular systems. In this work, we address this issue by the development of a novel theoretical framework that relies on the segregation of an ansatz into a dynamically selected core “*principal*” component, which is, by construction adiabatically decoupled from the remaining operators. This enables us to perform computations involving the *principal* component using extremely shallow-depth circuits whereas, the effect of the remaining “*auxiliary*” component is folded into the energy function via a cost-efficient non-iterative correction, ensuring the requisite accuracy. We propose a formalism that analytically predicts the *auxiliary* parameters from the *principal* ones, followed by a suite of non-iterative *auxiliary subspace correction* techniques with different levels of sophistication. The *auxiliary subspace corrections* incur no additional quantum resources, yet complement an inadequately expressive core of the ansatz to recover significant amount of electronic correlations. We have numerically validated the resource efficiency and accuracy of our formalism with a number of strongly correlated molecular systems.

I. INTRODUCTION

Quantum computing algorithms have recently garnered significant attention as they show immense promise to solve certain classically intractable many-body problems. Quantum computers leverage the principles of superposition and entanglement to bypass exponential or higher order polynomial scaling that existing classical electronic structure methods^{1–8} suffer from. Quantum phase estimation (QPE)^{9,10} was one of the first algorithms to theoretically showcase the quantum advantage. However, it suffers from deep quantum circuits, which results in huge accumulation of noise and extremely erroneous results when implemented using the currently available noisy intermediate scale quantum (NISQ) computers¹¹. To bypass this, hybrid quantum-classical algorithms like variational quantum eigensolver (VQE)¹² in the unitary coupled cluster (UCC) framework have recently gained immense popularity as they work by evaluating expectation values of parameterized operators in a quantum processing unit while the parameter optimization is outsourced to classical optimizers.

Another class of algorithm known as the projective quantum eigensolver (PQE)¹³ takes a different approach by optimizing the parameters using coupled cluster-like residual constructions. PQE can converge to identical energy values as that of VQE with similar or fewer quantum resources. It also shows inherent resilience to hard-

ware noise. These algorithms can be applied to simulate chemical systems in tandem with several error mitigation strategies^{14–19} to combat different sources of hardware errors for practical applicability. However, the scalability of VQE or PQE for dealing with larger molecular systems is restricted due to hardware limitations of NISQ devices and fundamental constraints of the error mitigation strategies²⁰. This necessitates the development of algorithms that can reduce the resource requirements of a given ansatz with reduced circuit complexity for less impact of noise while maintaining the characteristic accuracy as that of the original ansatz. Along this line, several algorithms have recently been developed in both VQE and PQE framework such as measurement-based iterative ansatz compactification methods^{21–32}, machine-learning based resource-efficient methods^{33–36}, qubit-space based CNOT reduction techniques^{37–40}, effective-Hamiltonian driven downfolding methods^{41–45}, methods of moments coupled cluster (MMCC^{46,47}) inspired quantum algorithms^{48–50} and measurement-free dimensionality reduction via many-body perturbative methods^{51,52} to mention some of them. Most of these methods rely upon a threshold based selection of a reduced subspace containing “important” operators. Properly tuned inclusion conditions on the threshold can enhance accuracy but lead to more complex circuits, which are often impractical for molecular applications in the NISQ era. Contrarily, a somewhat less stringent inclusion criteria compromises accuracy by selecting fewer important operators although it results in shallower circuits. Owing to the current hardware limitations, such shallower circuits are desired even though the corresponding compact

^{a)}Electronic mail: rmailto@chem.iitb.ac.in

ansatz is often not expressive enough for accurate energy calculations since it is attributed to only a relatively small number operators.

In this work, we address this problem by presenting a theoretical formalism that enables one to recover accurate electronic correlations even with such inadequately expressive dynamic ansatz. In this study, we have considered selected PQE (SPQE)¹³ as the dynamic selection protocol, which performs quantum measurements and iteratively picks up the important operators based on a threshold. Here we have shown that SPQE implicitly presumes a hierarchical structure among the parameters according to their convergence behavior which conforms to the *adiabatic approximation*^{51,53–55}, previously introduced by some of the present authors. It ensures a decoupling of the parameter space into a dominant, slower converging *principal parameter subset (PPS)* which is dynamically selected and optimized via SPQE. The leftover submissive, faster-converging parameters are collectively called the *auxiliary parameter subset (APS)*. Owing to this adiabatic decoupling, the corresponding operator space can be divided into a *principal* unitary subspace which forms the core of the ansatz and an *auxiliary* subspace. This particular structure of the unitary allows us to define an Adiabatically Decoupled UCC (AD-UCC) ansatz, which plays a central role in the entire analysis. We have further developed a mathematical framework that predicts the leftover *auxiliary* parameters from the SPQE-driven *principal* parameters. This inter-relationship between the *principal* and *auxiliary* parameters is established based on our recently developed *slaving principle* in the framework of nonlinear electronic structure optimization problems in both classical^{53,54,56,57} and quantum^{51,55} computing parlance. Further, the effect of the *auxiliary* parameters is folded into the energy functional in an approximate manner via non-iterative *auxiliary subspace corrections* (ASC) without the need for any additional circuit resources. The advantage of our method is particularly more pronounced with less accurate core ansatz where ASC effectively complements the core for a dramatic improvement of the energy accuracy at an extremely reduced circuit depth. Since the algorithm enforces adiabatic decoupling through SPQE with a posteriori ASC, we refer to this algorithm as AD(SPQE)-ASC. Though we have considered SPQE framework here for the analysis, adiabatic decoupling is a general formalism and can be extended to other dynamic algorithms as well. To numerically establish the efficacy of our method, we have studied the relative performances of SPQE and AD(SPQE)-ASC with different levels of non-iterative approximations for challenging molecular cases such as stretching of linear H_4 , linear H_6 and symmetric stretching of $O-H$ bond in H_2O which are considered to be prototypical models for electronic strong correlation effects.

The manuscript is structured as follows, we start with the preliminary discussion on PQE and SPQE. Then we move over to the mathematical formalism of AD(SPQE)-

ASC which contains efficient *principal* parameter selection, predicting the *auxiliary* parameters from the *principal* ones and designing different variants of post-optimization non-iterative corrections to the energy function. Subsequently, we present our numerical results to establish the superiority of the algorithm.

II. THEORY

A. Selected Projective Quantum Eigensolver and the Spontaneous Emergence of Adiabatic Decoupling Conditions

The ground state of a molecular Hamiltonian can be approximated by disentangled unitary coupled cluster⁵⁸ (dUCC) ansatz $|\Psi\rangle = \hat{U}(\boldsymbol{\theta})|\Phi_0\rangle$ parameterized by $\boldsymbol{\theta}$, where $|\Phi_0\rangle$ is the Hartree-Fock (HF) reference state and \hat{U} is taken to be

$$\hat{U}(\boldsymbol{\theta}) = \prod_{\mu} e^{\theta_{\mu} \hat{\kappa}_{\mu}} \quad (1)$$

where, $\hat{\kappa}_{\mu} = \hat{\tau}_{\mu} - \hat{\tau}_{\mu}^{\dagger}$ is an anti-Hermitian operator with $\hat{\tau}_{\mu} = \hat{a}_a^{\dagger} \hat{a}_b^{\dagger} \dots \hat{a}_j \hat{a}_i$ and the boldface $\boldsymbol{\theta}$ represents the parameter vector. Here, μ represents a multi-index particle-hole excitation structure as defined by the string of creation (\hat{a}^{\dagger}) and annihilation (\hat{a}) operators with the indices $\{i, j, \dots\}$ denoting the occupied spin-orbitals in the HF state and $\{a, b, \dots\}$ denoting the unoccupied spin-orbitals. Since all the unitary operators are parameterized, we will interchangeably use the words “operator” and “parameters” depending on the context. In PQE¹³ framework the parameters that satisfy the Schrodinger equation can be obtained by iterative optimization via $\theta_{\mu}^{(m+1)} = \theta_{\mu}^{(m)} + \frac{r_{\mu}^{(m)}}{D_{\mu}}$ where, m is the iterative step counter and D_{μ} is the Møller-Plesset denominator. Here, r_{μ} is the residual element constructed by taking projections against excited determinants $|\Phi_{\mu}\rangle$

$$r_{\mu}(\boldsymbol{\theta}) = \langle \Phi_{\mu} | \hat{U}^{\dagger}(\boldsymbol{\theta}) \hat{H} \hat{U}(\boldsymbol{\theta}) | \Phi_0 \rangle ; \mu \neq 0. \quad (2)$$

The residuals can be efficiently calculated using a quantum computer as they can be expressed as a sum of diagonal quantities¹³

$$r_{\mu} = \langle \Omega_{\mu}(\pi/4) | \bar{H} | \Omega_{\mu}(\pi/4) \rangle - \frac{1}{2} E_{\mu} - \frac{1}{2} E_0 \quad (3)$$

with the following definitions, $|\Omega_{\mu}(\theta)\rangle = e^{\hat{\kappa}_{\mu} \theta} |\Phi_0\rangle$, $\bar{H} = \hat{U}^{\dagger} \hat{H} \hat{U}$, $E_{\mu} = \langle \Phi_{\mu} | \bar{H} | \Phi_{\mu} \rangle$ and $E_0 = \langle \Phi_0 | \bar{H} | \Phi_0 \rangle$. Due to the exponential parameterization of the ansatz and the non-terminating nature of the BCH expansion stemming from the non-commutativity of the anti-Hermitian $\hat{\kappa}_{\mu}$ operators, the optimization is highly coupled and nonlinear in nature. In such an iterative optimization problem, one may implicitly introduce the notion of discrete-time which may be assumed to be embedded in each iteration step, as often done in studying nonlinear *iterative*

maps⁵⁹. Thus, this iteration step “ m ” is to be taken as discrete time step such that the variation of the parameters in two subsequent iterations can be expressed as

$$\Delta\theta_\mu^{(m)} = \frac{r_\mu^{(m)}}{D_\mu} \quad (4)$$

where, $\Delta\theta_\mu^{(m)} = \theta_\mu^{(m+1)} - \theta_\mu^{(m)}$ with m being the iteration number. The iterative procedure is deemed converged when the residual condition

$$r_\mu \rightarrow 0 \quad (5)$$

is satisfied. For PQE with n -tuple excitation operators, the iterative procedure requires the construction and optimization of $(n_o n_v)^n$ residue elements which often leads to deep quantum circuits. A more lucrative alternative is to dynamically select only a handful of operators that are important (such that the gate depth can be kept low) for a specific molecule and specific nuclear arrangement at the cost of additional quantum measurements. It can be done with selected PQE (SPQE)¹³ which starts with an operator pool and consists of two sets of iterative cycles, namely *macro-iterations* for selecting the important operators from the pool and *micro-iterations* to optimize the corresponding parameters. At k -th macro-iteration, a *residual state* defined as

$$\begin{aligned} |\tilde{r}^{(k)}\rangle &= (1 + i\Delta t \hat{U}^\dagger(k) \hat{H} \hat{U}(k)) |\Phi_0\rangle \\ &= C_0^{(k)} |\Phi_0\rangle + \sum_\mu C_\mu^{(k)} |\Phi_\mu\rangle \end{aligned} \quad (6)$$

is constructed, where $\hat{U}^{(k)}$ consists of all the selected operators in the previous 0 to $(k-1)$ macro-iterations. The coefficients $C_\mu^{(k)}$ are proportional to the residuals $r_\mu^{(k)} = \hat{U}^\dagger(k) \hat{H} \hat{U}(k)$ and given by approximately¹³ $|C_\mu^{(k)}| \approx \Delta t |r_\mu^{(k)}|$ where Δt is the evolution time which is in general small in magnitude. The residual state is measured to get a probability distribution of the excited determinants $|\Phi_\mu\rangle$. From the entire operator pool, those operators are excluded that have the summation of their residual squared less than the square of a pre-defined macro-iteration threshold Ω , such that

$$\sum_{\mu}^{\text{excluded}} |r_\mu^{(k)}|^2 \approx \sum_{\mu}^{\text{excluded}} \frac{|C_\mu^{(k)}|^2}{\Delta t^2} \leq \Omega^2 \quad (\text{exclusion criteria}) \quad (7)$$

The remaining excitation operators are then selected at k -th macro-iteration, optimized using PQE micro-iteration cycles (which uses Eq. (4)) and appended to $\hat{U}^{(k)}$ for generating the residual state in the next $(k+1)$ -th iteration via Eq. (6) till all the unique operators to be added are exhausted. Thus, using an alternate combination of macro and micro iterations, SPQE can construct a dUCC ansatz sequence consisting of only “important” operators.

The discussions so far suggest that the selection of operators in SPQE is entirely dependent upon the macro-iteration threshold (Ω). SPQE can be made systematically more accurate by tuning Ω to include more operators into the ansatz, however, at the cost of increased circuit depth. To circumvent this, we introduce a mathematical framework here requiring minimal gate-depth SPQE computations on a quantum processor that can cater to the needs of modern NISQ devices. In addition to that, a set of non-iterative energy corrections complements for the lost correlation, ensuring the requisite accuracy of the problem. Towards this development, we borrow some of the ideas from our recent works^{51,55} that establishes that there exists an explicit hierarchy regarding the *convergence timescale* (or, number of iterations required for convergence) of the parameters which enables an adiabatic decoupling of the entire operator space into a dominant *principal* and a submissive *auxiliary* subpart having different timescale of equilibration. We argue and demonstrate that a problem-specific and dynamically flexible *principal-auxiliary* decoupling, which has profound mathematical consequences towards efficiency and efficacy (*vide infra*), spontaneously emerges from SPQE as follows:

- It is evident from Eq. (4) that the parameter variation is solely dictated by the magnitude of the associated residual

$$\Delta\theta_\mu \propto r_\mu. \quad (8)$$

Since operator exclusion/inclusion criteria (Eq. (7)) explicitly depends upon the absolute magnitude of the residuals r_μ , this proportionality condition (Eq. (8)) immediately ensures that the parameters selected via SPQE are usually those that take much more time (iteration steps) to converge (in a conventional PQE) owing to the larger magnitude of the associated residual. These parameters span the *PPS* and are denoted as $(\theta_P^{(SPQE)})$ since this subset is constructed via SPQE measurements. The number of elements in this space is N_P . Due to their importance from a many-body perspective, this subspace form the core of the bipartitely decoupled ansatz.

- The complementary operator pool that satisfies the exclusion criteria (Eq. (7)), are not selected in the core, owing to its smaller magnitude of the residuals and consequently faster timescale of equilibration. The associated parameters span the *APS* with the corresponding number of elements denoted by N_A . Therefore, the whole parameter set ($\{\theta\}$) can now be divided into *principal* and *auxiliary* parameters such that:

$$\{\theta\} = \{\theta_P^{(SPQE)}\} \oplus \{\theta_A\} \quad (9)$$

The smaller relative magnitude of the residual elements for the excluded parameters ensures that the

absolute magnitude of the *principal* parameters are significantly larger than that of the *auxiliary* ones

$$|\theta_P^{(SPQE)}| \gg |\theta_A|. \quad (10)$$

To translate this notion of parameter space segregation into the operator space, we can define a *principal-auxiliary bipartite unitary* operator (\hat{U}_{pab}) such that

$$\hat{U}_{pab} = \hat{U}_P(\boldsymbol{\theta}_P^{(SPQE)}) \cdot \hat{U}_A(\boldsymbol{\theta}_A) \quad (11)$$

where, $\hat{U}_P(\boldsymbol{\theta}_P^{(SPQE)})$ and $\hat{U}_A(\boldsymbol{\theta}_A)$ are *principal* and *auxiliary* unitary operators, respectively, each possessing the disentangled form as defined in Eq. (1). For notational convenience we will henceforth denote $\boldsymbol{\theta}_P^{(SPQE)}$ as $\boldsymbol{\theta}_P$. This particular structure of the unitary leads to the following form of the associated correlated state

$$|\Psi_{AD-UCC}\rangle = \hat{U}_{pab} |\Phi_0\rangle = e^{\hat{\kappa}_P \boldsymbol{\theta}_P} e^{\hat{\kappa}_A \boldsymbol{\theta}_A} |\Phi_0\rangle \quad (12)$$

which we term as the Adiabatically Decoupled UCC (AD-UCC) ansatz. The ordering of \hat{U}_{pab} is such that the Hamiltonian transformation begins with the largest many-body rotation and continues in a descending manner

$$\begin{aligned} H &\rightarrow \hat{U}_A^\dagger \cdot \hat{U}_P^\dagger \hat{H} \hat{U}_P \cdot \hat{U}_A \\ &= \dots e^{-\theta_{A\mu_2} \hat{\kappa}_{A\mu_2}} e^{-\theta_{A\mu_1} \hat{\kappa}_{A\mu_1}} \dots e^{-\theta_{P\mu_2} \hat{\kappa}_{P\mu_2}} e^{-\theta_{P\mu_1} \hat{\kappa}_{P\mu_1}} \\ &\hat{H} e^{\theta_{P\mu_1} \hat{\kappa}_{P\mu_1}} e^{\theta_{P\mu_2} \hat{\kappa}_{P\mu_2}} \dots e^{\theta_{A\mu_1} \hat{\kappa}_{A\mu_1}} e^{\theta_{A\mu_2} \hat{\kappa}_{A\mu_2}} \dots \end{aligned} \quad (13)$$

where, $|\theta_{P\mu_1}| > |\theta_{P\mu_2}| \dots > |\theta_{A\mu_1}| > |\theta_{A\mu_2}| \dots$ and so on with subscript P (A) denoting the elements of the *principal* (*auxiliary*) subspace. One may of course design an energy function where the *auxiliary* parameters are neglected altogether, which is referred to as SPQE energy function

$$E_{SPQE} = \langle \Phi_0 | \hat{U}_P(\boldsymbol{\theta}_P) \hat{H} \hat{U}_P(\boldsymbol{\theta}_P) | \Phi_0 \rangle. \quad (14)$$

Such an ansatz where only θ_P s are included can be made arbitrarily accurate as mentioned earlier by tuning Ω to exclude less and involve more number of operators (and parameters) into \hat{U}_P . This, however, leads to a rapid proliferation of the associated circuit depth. Therefore, in the NISQ era, it is desirable to develop algorithms that can maintain the requisite accuracy even with extremely compact core ansatz to improve scalability. In such a scenario, the *auxiliary* counterpart \hat{U}_A , which is completely ignored in the above expression (Eq. (14)), can have important contributions to the correlation energy specially in the strongly correlated regime. With an in-built recipe for adiabatic decoupling by SPQE, in the next section we develop a framework that provides the posteriori energy correction to factor in the *auxiliary* operators without any additional major quantum resources.

B. Synergistic Mapping of the Auxiliary Parameters and Non-iterative Auxiliary Subspace Corrections to Energy

The discussions of section II A suggest that *principal* parameters obtained from SPQE with appropriate conditions on Ω are pivotal for accurate energy predictions of a molecular system. However, for a resource-efficient implementation of SPQE, we need to judiciously incorporate the larger *auxiliary* subspace into the energy function. This is required to complement the inadequately parameterized compact ansatz and retrieve the electronic correlation. Towards this, we can invoke the *adiabatic approximation*^{51,53–55,60,61} which allows us to neglect the variation of *auxiliary* parameters in successive iterations

$$\Delta\theta_{A_\alpha} = 0 \quad (\text{adiabatic approximation}) \quad (15)$$

since it converges significantly faster than the *principal* parameters. Along with this approximation, the condition in Eq. (10) can be utilized to design a mathematical function that predicts the *auxiliary* parameters from the information regarding the optimized *principal* parameters only. This is executed via computing the residual-like matrix elements of the similarity transformed Hamiltonian $\hat{U}_P^\dagger \hat{H} \hat{U}_P$ projected against the *auxiliary*-space excited determinants (see Appendix A for detailed steps)

$$\theta_{A_\alpha} = \frac{1}{D_{A_\alpha}} \langle \Phi_{A_\alpha} | \hat{U}_P^\dagger(\boldsymbol{\theta}_P) \hat{H} \hat{U}_P(\boldsymbol{\theta}_P) | \Phi_0 \rangle \quad (16)$$

which can be efficiently implemented on a quantum computer by expanding it in terms of three diagonal expectation values as shown in Eq. (3). The expression for *principal-to-auxiliary mapping* in Eq. (16) is a general equation that gives us an accurate estimate of the *auxiliary* parameters where the coupling between the *principal* and *auxiliary* parameters are switched off during the optimization of the former. In general this mapping is done as a single step procedure only after the *principal* parameters are optimized.

However, the explicit computation of the matrix elements may potentially be bypassed particularly for SPQE-based adiabatic decoupling. This is due to the fact that at the last macro-iteration ($k = k_{max}$) cycle $\hat{U}^{(k_{max})} = \hat{U}_P$ (see Eq. (6), (7)) and the matrix element in Eq. (16) is equivalent to those r_μ 's which remain excluded. One may of course construct the matrix elements explicitly upon the dynamic selection of the *principal* parameters using any method of choice other than SPQE, which may incur nominal measurement overhead as will be discussed shortly. Further, with the criteria that the *auxiliary* parameters are in general smaller in magnitude (Eq. (10)), the energy function can be approximated in a way that contains the effect of larger many-body rotations via *principal* parameters exactly and folds in the effect of the *auxiliary* parameters approximately as correction terms with the second-order truncation of the

Baker-Campbell-Hausdorff (BCH) expansion

$$\begin{aligned}
E &= \langle \Phi_0 | \hat{U}_A^\dagger \hat{U}_P^\dagger \hat{H} \hat{U}_P \hat{U}_A | \Phi_0 \rangle \\
&\approx \underbrace{\langle \Phi_0 | \bar{H}_P | \Phi_0 \rangle}_{E_{SPQE}} + \underbrace{\sum_{A_\alpha \in APS} \theta_{A_\alpha}(\boldsymbol{\theta}_P) \langle \Phi_0 | [\bar{H}_P, \hat{\kappa}_{A_\alpha}] | \Phi_0 \rangle}_{\text{Term 1}} \\
&+ \underbrace{\frac{1}{2} \sum_{A_\alpha, A_\beta} \theta_{A_\alpha}(\boldsymbol{\theta}_P) \theta_{A_\beta}(\boldsymbol{\theta}_P) \langle \Phi_0 | [[\bar{H}_P, \hat{\kappa}_{A_\alpha}], \hat{\kappa}_{A_\beta}] | \Phi_0 \rangle}_{\text{Term 2}}
\end{aligned} \tag{17}$$

where, $\bar{H}_P = \hat{U}_P^\dagger \hat{H} \hat{U}_P$. Note that, in this context the particular structure of the *principal-auxiliary bipartite* operator \hat{U}_{pab} (Eq. (11)) is extremely important in attaining the approximate energy function here. In the above expression *Term 1* and *Term 2* are only added after the optimization, once we have access to the mapped *auxiliary* parameters via Eq. (16). Thus, these two terms are collectively referred to as the post-optimization non-iterative *auxiliary subspace correction* (ASC) terms. Computation of *Term 1* on a quantum computer is relatively straightforward as it can be evaluated analytically into the following expression (see Appendix C for detailed derivation)

$$\sum_{A_\alpha \in APS} \theta_{A_\alpha}(\boldsymbol{\theta}_P) \langle \Phi_0 | [\bar{H}_P, \hat{\kappa}_{A_\alpha}] | \Phi_0 \rangle = 2\theta_{A_\alpha}^2 D_{A_\alpha} \tag{18}$$

Evaluating *Term 2* exactly is particularly non-trivial and since it already contains nonlinearity, the BCH expansion of the similarity transformed Hamiltonian can be approximated to leading order bare Hamiltonian only, i.e. $\bar{H}_P \approx \hat{H}$. We then invoke the Møller-Plesset partitioning of the Hamiltonian with canonical spin orbitals such that the Hamiltonian can be written as $\hat{H} = \hat{F}^{(0)} + \hat{V}^{(1)}$, where $\hat{F}^{(0)} = \sum_q f_q \hat{a}_q^\dagger \hat{a}_q$ is the zeroth order one-body Fock operator with f_q being the one-body integrals and $\hat{V}^{(1)}$ is the first order two-body operator. *Term 2* can be approximated in two different ways and we refer to these two approximations as scheme-I and scheme-II (also represented as AD(SPQE)-ASC (I/II)). In scheme-I, only the zeroth order Fock operator is retained in the Hamiltonian and it leads to the following simplified energy expression

$$E^{(I)} = \underbrace{\langle \Phi_0 | \hat{U}_P^\dagger(\boldsymbol{\theta}_P) \hat{H} \hat{U}_P(\boldsymbol{\theta}_P) | \Phi_0 \rangle}_{E_{SPQE}} + \underbrace{\sum_{A_\alpha} \theta_{A_\alpha}^2 D_{A_\alpha}}_{ASC(I)} \tag{19}$$

It is interesting to note that the ASC term for scheme-I, which spontaneously emerges from the *adiabatic approximation* and *slaving principle*, shares some level of structural kinship to the non-iterative corrections stemming from method of moments CC (MMCC) theory^{47,48,62–64}. However, as one can see from the analysis so far, the mathematical origin and underlying approximations for moments corrections and ASC are fundamentally different. On the other hand, in scheme-II the full Hamiltonian

is retained and the energy expression becomes

$$\begin{aligned}
E^{(II)} &= \underbrace{\langle \Phi_0 | \hat{U}_P^\dagger(\boldsymbol{\theta}_P) \hat{H} \hat{U}_P(\boldsymbol{\theta}_P) | \Phi_0 \rangle}_{E_{SPQE}} + \\
&\underbrace{2 \sum_{A_\alpha} \theta_{A_\alpha}^2 D_{A_\alpha} + \frac{1}{2} \sum_{A_\alpha} \theta_{A_\alpha}^2 \langle \Phi_0 | [[H, \hat{\kappa}_{A_\alpha}], \hat{\kappa}_{A_\alpha}] | \Phi_0 \rangle}_{ASC(II)}
\end{aligned} \tag{20}$$

The detailed steps leading to the above expressions in Eq. (19) and (20) are shown in Appendix C. Thus, the benefit of this entire protocol is that one can obtain and optimize *principal* parameters via SPQE with a compact circuit while *auxiliary* parameters and energy are calculated using Eq. (16), (19) (scheme-I) and 20 (scheme-II) with the same shallow-circuit depth as that of SPQE since all the evaluations are constrained entirely to the *principal* subspace. The additional computations necessary for ASC in Eq. (19) and (20) (both scheme-I and II) is governed by the *principal-to-auxiliary mapping* (Eq. (16)) which in general requires $\dim\{APS\} = N_A$ number of extra residual element evaluations of the type $\langle \Phi_\mu | \hat{H} | \Phi_0 \rangle$. However, as discussed earlier in this section, for the particular case of SPQE, the mapping via Eq. (16) can be extracted from the SPQE selection protocol itself. Thus specifically for SPQE, ASC does not require any additional residue evaluations which saves a significant amount of computational overhead. Scheme-II further requires some nominal amount of measurements stemming from the last term of Eq. (20) for a better approximation. Note that this extra measurements for scheme-II do not involve any circuits with unitary operators and are significantly less than the overall SPQE measurement cost (see Appendix D for details). Since the adiabatic decoupling is obtained via SPQE and it includes a non-iterative ASC for energy, we term this formalism as AD(SPQE)-ASC that consists of the following steps-

- *Principal Parameter Selection and Optimization:* SPQE is performed by the construction of residual state (Eq. (6)) at k -th macro-iteration and the important operators are filtered according to the condition in Eq. (7). The corresponding parameters are optimized using micro-iteration cycles via Eq. (4) and appended to $\hat{U}^{(k)}$ to form $\hat{U}^{(k+1)}$. This updated unitary is used to form the residual state at $(k+1)$ -th step and the entire protocol involving macro and micro-iterations continues. When no new operators are added to the unitary, SPQE terminates and we have an ordered and optimized set of operators which can be taken to be the *PPS*.
- *Post-Optimization Principal-to-Auxiliary Mapping:* The leftover operators not taken into the ansatz by SPQE form the *APS*. These *auxiliary* parameters are mapped from the *principal* parameters via the relationship established in Eq. (16).

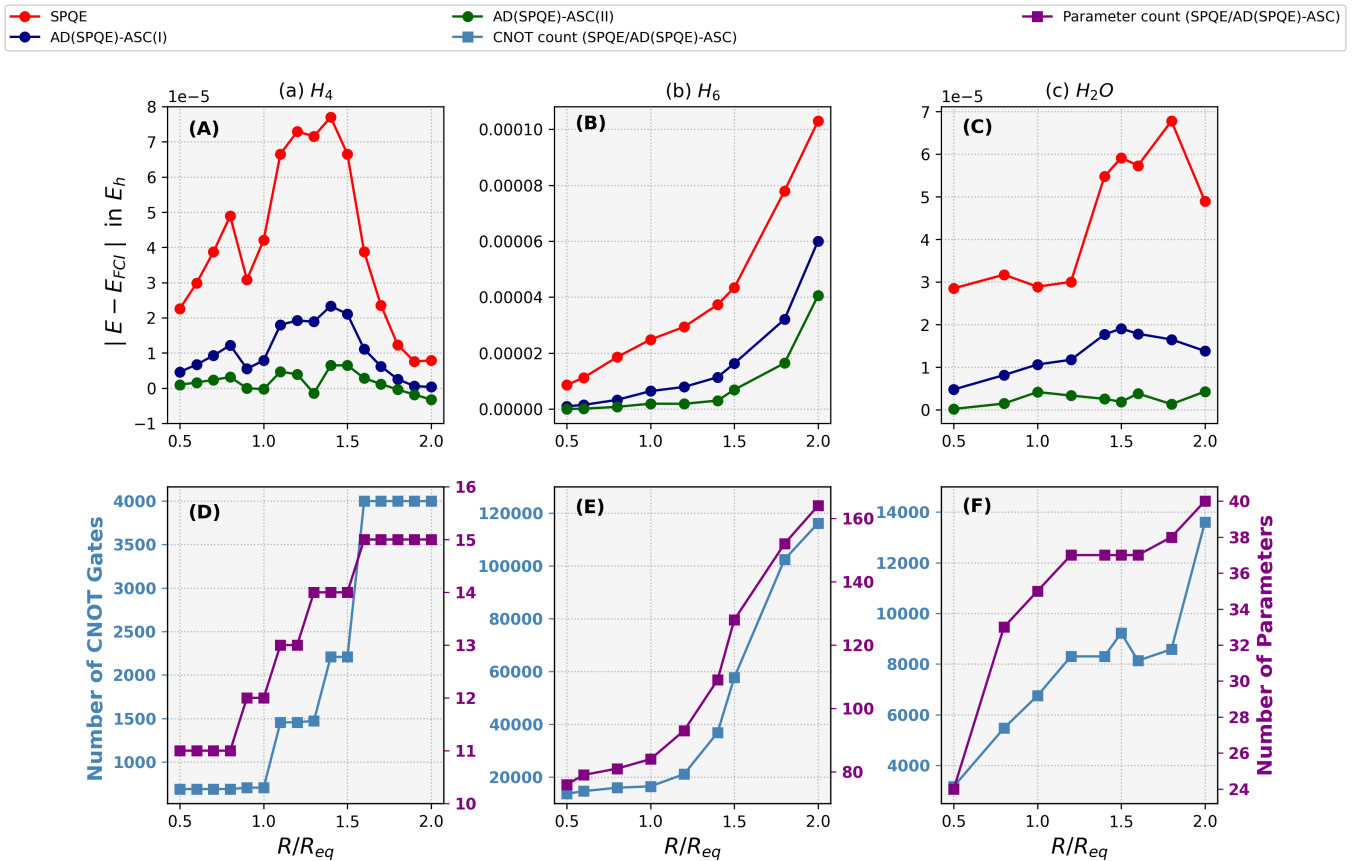


FIG. 1. Comparison between SPQE and AD(SPQE)-ASC (scheme-I and II) for bond stretching of linear (a) H_4 and (b) H_6 chains and (c) symmetric stretching of H_2O with the information regarding the molecular geometries given in section III. SPQE and AD(SPQE)-ASC contain up to quadruples excitation operators in the pool. The first row ((A), (B), (C)) represents the energy error with respect to FCI over the potential energy surface. In the second row ((D), (E), (F)) we show the CNOT counts and parameter counts (in the twin y-axis) along various nuclear arrangements for SPQE and AD(SPQE)-ASC. Note that for a given Ω , both the methods require the same quantum resources.

- *Non-iterative Correction to Energy:* The final energy is obtained using the expressions Eq. (19) for scheme-I and Eq. (20) for scheme-II.

In the next section we will discuss the accuracy and efficiency of this algorithm for challenging molecular applications.

III. RESULTS AND DISCUSSION

In this section we will illustrate the numerical results of our theoretical development by comparing AD(SPQE)-ASC (scheme I and II) with SPQE. The numerical studies were performed with an in-house python code implemented by interfacing QForte⁶⁵ and Qiskit⁶⁶. For the analysis we have studied the ground state potential energy surface (PES) for (a) linear H_4 (equilibrium distance $R_{(eq)H-H} = 0.75\text{\AA}$), (b) linear H_6 ($R_{(eq)H-H} = 0.75\text{\AA}$) and (c) symmetric $O-H$ bond stretching of H_2O

molecule ($R_{(eq)O-H} = 0.958\text{\AA}$, $\angle H-O-H = 104.4776^\circ$ with frozen core approximation) which are considered to be standard systems to study the electronic strong-correlation behaviour. We have used STO-3G basis set for all our calculations with the electronic integrals imported from PySCF⁶⁷ driver in Qiskit and from Psi4⁶⁸ in QForte. The fermion-to-qubit mapping of the Hamiltonian is done using Jordan-Wigner⁶⁹ transformation. For all our studies, SPQE operator selection and energy calculation is done by QForte with micro-iteration convergence threshold 10^{-5} and $\Delta t = 0.001$. The selected excitation operators are then mapped to Qiskit convention for the computation of ASC. All the methods under consideration contains singles, doubles, triples and upto quadruples (SDTQ) excitations unless mentioned otherwise.

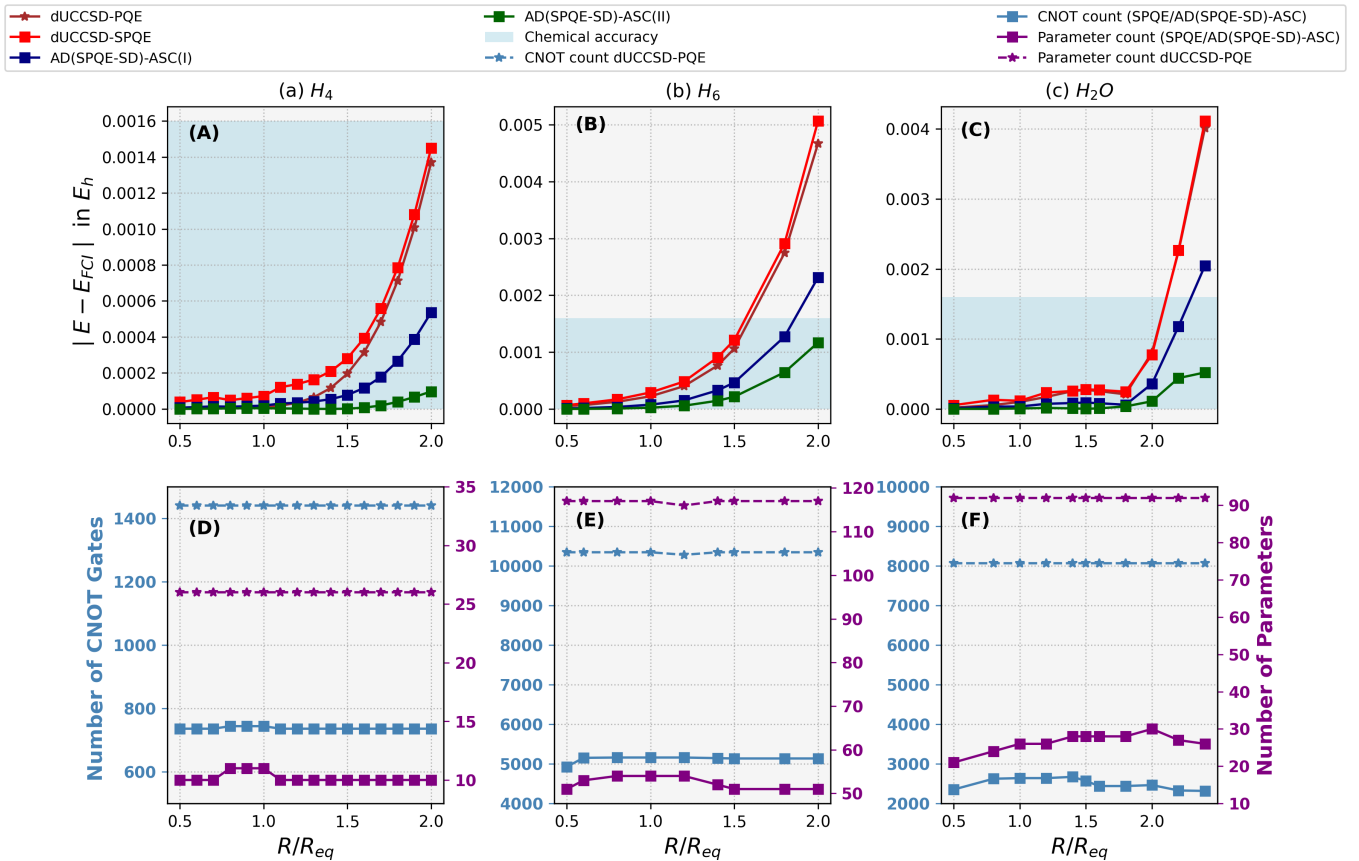


FIG. 2. Comparison between dUCCSD-SPQE and AD(SPQE-SD)-ASC (scheme-I and II) for bond stretching of linear (a) H_4 and (b) H_6 chains, and (c) symmetric stretching of H_2O . For comparison, the conventional dUCCSD-PQE results are also plotted. First row ((A), (B), (C)) shows the energy difference from FCI against the different geometrical arrangements of the molecules. The second row ((D), (E), (F)) shows CNOT and parameter counts for the corresponding molecular configurations.

A. Accuracy over the potential energy profile of strongly correlated chemical systems:

In order to substantiate the effects of ASC in ideal conditions, Fig. 1 shows the comparison between AD(SPQE)-ASC and standard SPQE implementation with the macro-iteration threshold (Ω) taken to be 10^{-2} . In Fig. 1 ((A), (B), (C)) we have plotted the energy difference from Full Configuration Interaction (FCI) (in E_h) along the y-axis and the ratio ($\frac{R}{R_{eq}}$) along the x-axis where, R is the bond distance and R_{eq} is the equilibrium distance. For all the molecular cases AD(SPQE)-ASC (both scheme-I and II) shows better accuracy than SPQE while having the same circuit depth, specifically with stretched geometries where the strong electronic correlations prevail. For example in Fig. 1(B) we can see that in the case of H_6 with $\frac{R}{R_{eq}} = 2.0$ the energy error with respect to FCI for SPQE is $\sim 0.11 mE_h$ while that of scheme-II is $\sim 0.04 mE_h$, providing almost one order-of-magnitude better energy accuracy as compared to SPQE. The results suggest that scheme-II is the most accurate of

all since it contains the additional commutator correction terms (Eq. (20)). The CNOT count and parameter count (for the circuits corresponding to $\tilde{U}_P(\theta_P)|\Phi_0\rangle$) are represented in Fig. 1 ((D), (E), (F)) with color codes blue and purple respectively. Here, we must re-iterate that AD(SPQE)-ASC does not require any additional circuit resources and the CNOT gate count and number of parameters as shown in all the plots remain exactly the same for both SPQE and our method.

However, as evident from Fig. 1, since the operator pool contains SDTQ excitations, the CNOT counts even for SPQE at stretched geometries proliferates excessively to account for the electronic correlation via including triples and quadruple excitation operators into the core of the ansatz. For example, the CNOT count for H_6 (Fig. 1(E)) reaches around 10^5 for the stretched geometries which is way beyond the hardware capabilities of the near term quantum computers. Thus there is a pressing need to develop methods that can attain chemically accurate description of such challenging molecular applications with less utilization of the quantum circuit resources. Regarding this, in subsection III B we discuss

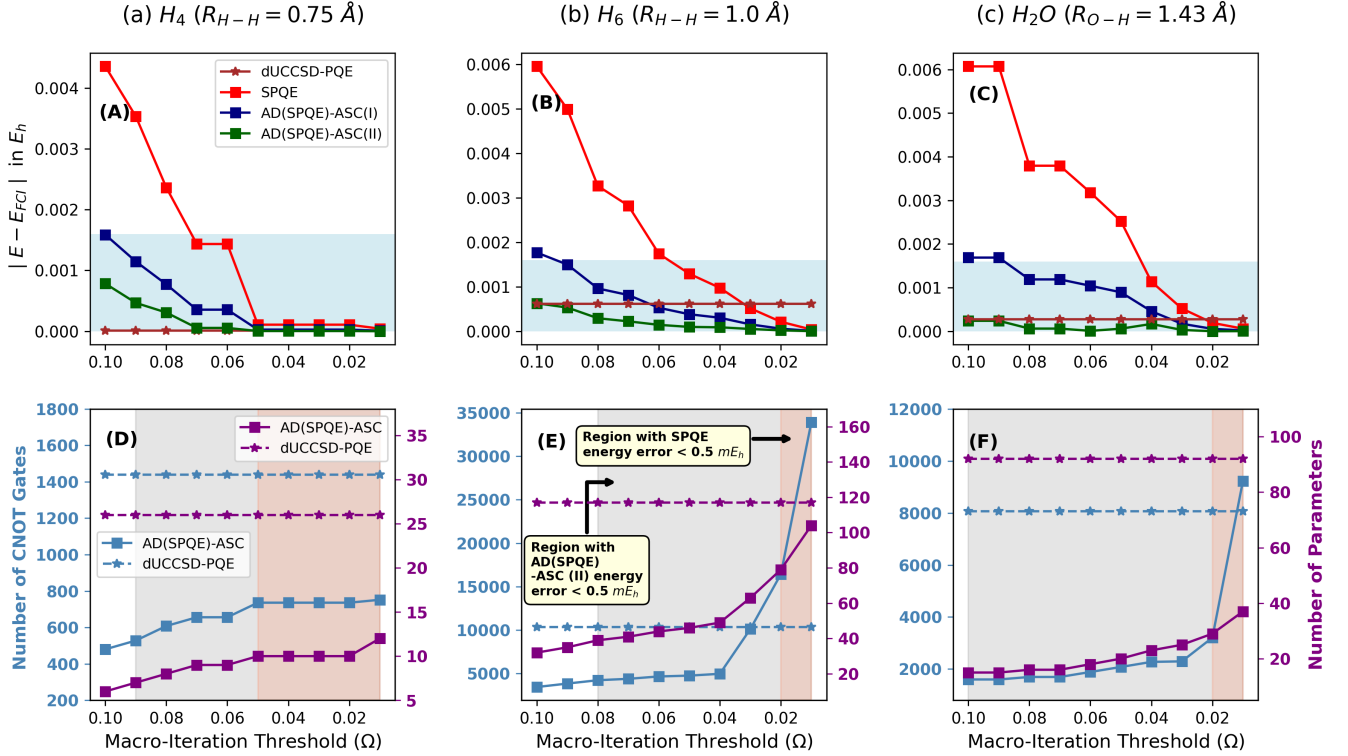


FIG. 3. Comparison between SPQE, AD(SPQE)-ASC (scheme-I and II) (with SDTQ pool) with different macro-iteration threshold (Ω) and dUCCSD-PQE for near equilibrium geometries of (a) H_4 , (b) H_6 and (c) H_2O with the bond distances mentioned in each column. Here (A), (B) and (C) represent the absolute energy error with respect to FCI for different values of Ω . Subplots (D),(E), (F) represent the number of CNOT gates (with parameter counts in a twin axis). The gray and red shaded areas in (D)-(F) show the range of the Ω where the energy difference lies below $0.5 mE_h$ with respect to FCI for AD(SPQE)-ASC (II) and SPQE, respectively. In general AD(SPQE)-ASC enters the gray region with much less number of CNOT (and parameter) counts than SPQE which represents that for achieving a similar accuracy (in this case $0.5 mE_h$), the former requires significantly less quantum resources due to additional ASC.

how AD(SPQE)-ASC can provide us with a mechanism to attain chemical accuracy utilizing minimal quantum resources.

B. Numerical Estimation of Resource Efficiency

The results from section III A suggest that selection of operators from SDTQ operator pool can cause an excessive increase in circuit depth to an impractical level considering the current NISQ devices. This can be modulated by tuning Ω to restrict the operators that are included in the core of the ansatz. Moreover, at a lower threshold ($\Omega \sim 0.01$), AD(SPQE)-ASC and SPQE would be of similar order of accuracy in all cases as lower thresholds typically suggest a more exhaustive inclusion of the parameters into the core of the ansatz, leaving almost no room for a discernible improvement via ASC. Thus the most significant advantage of ASC is pronounced for the following two cases:

1. Attaining chemical accuracy with SPQE operator pool restricted to singles and doubles:

In order to keep the gate depth as shallow as possible, we restrict the core of the ansatz formed by only SD operators from a pool of SDTQ, while the energy corrections due to the remaining SD and all TQ operators are embedded via ASC. We refer to this variant as AD(SPQE-SD)-ASC to explicitly represent the operator pool type (in this case SD) considered in SPQE. In Fig. 2 we have shown the numerical comparisons between SPQE, AD(SPQE)-ASC and dUCCSD-PQE for the potential energy surfaces of all the molecules under consideration. The blue shaded area shows the chemical accuracy energy window ($\sim 1.6 mE_h$ energy error from FCI). In case of linear H_6 (Fig. 2(B), (E)) scheme-II outperforms all the other methods while maintaining the chemical accuracy throughout the PES, with CNOT count as low as ~ 5000 even for stretched geometries compared to the gate count $\sim 10^5$ with SDTQ pool (Fig. 1(E)). One may note that in all these cases both dUCCSD-PQE and dUCCSD-SPQE fail to account for the strong

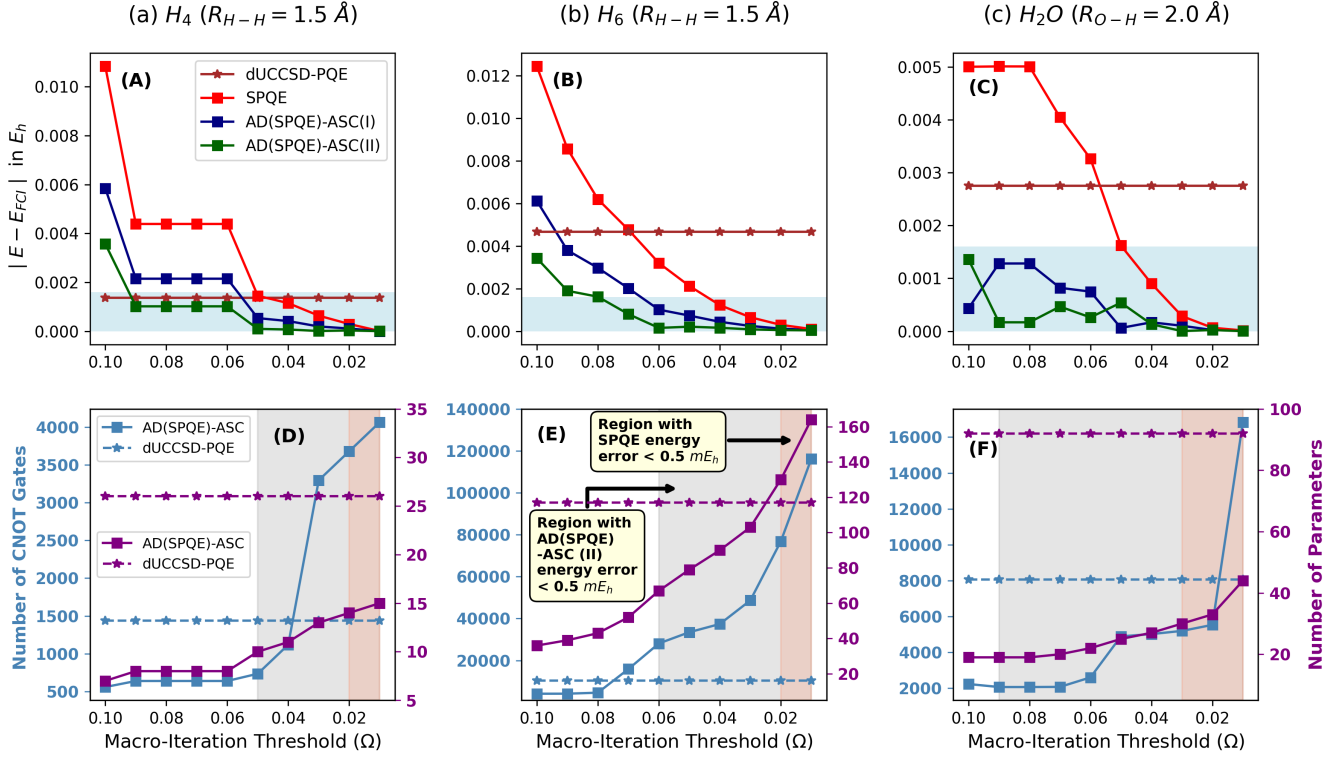


FIG. 4. Comparison between SPQE, AD(SPQE)-ASC (scheme-I and II) (with SDTQ pool) and dUCCSD-PQE with different macro-iteration threshold (Ω) for stretched geometries of (a) H_4 , (b) H_6 and (c) H_2O with the bond distances mentioned above each column. For other details, see Fig. 3.

correlation at stretched geometries. AD(SPQE-SD)-ASC complements such incomplete inclusion of correlation via ASC to account for the missing SD and all TQ effects and attains chemical accuracy for all the cases in our study, albeit with quantum resources equal to that of dUCCSD-SPQE.

2. Resource Efficient Performance with higher macro-iteration threshold:

In general, SPQE demonstrates systematically more accurate results as Ω is adjusted from higher to lower values at the cost of increased quantum resource utilization. In this regard, we aim to highlight the significantly improved accuracy that AD(SPQE)-ASC provides compared to SPQE via non-iterative ASC even at higher Ω values. This is shown in Fig. 3 and Fig. 4 for equilibrium and stretched geometries of linear H -chain (column (a) H_4 and column (b) H_6 with $R_{H-H} = 0.75 \text{ \AA}$, 1.5 \AA) and H_2O (column (c) with $R_{O-H} = 1.43 \text{ \AA}$, 2.0 \AA) respectively. These comparisons between SPQE and AD(SPQE)-ASC (both scheme I and II) involve varying Ω from 0.1 to 0.01 along the x-axis, with the energy difference from FCI plotted in the y-axis in the first row of both Fig. 3 and 4 (labeled as (A), (B) and (C)). For reference, dUCCSD-PQE results are also shown on the

same scale. In the second row of Fig. 3 and 4 ((D), (E), (F)) we have shown the CNOT count (the corresponding parameter count shown in a twin axis) which are, as previously discussed, same for both SPQE and AD(SPQE)-ASC. The corresponding grey and pink shaded areas are to highlight the region where AD(SPQE)-ASC and SPQE energies are within $0.5 mE_h$ from FCI, respectively.

The results from numerical simulations in Fig. 3, 4 shows that for all the molecules, AD(SPQE)-ASC (both scheme I and II) outperforms SPQE in terms of accuracy and resource efficiency. It can be observed from the plots that with higher Ω (~ 0.1), SPQE selects only a small number of dominant operators from the pool which is unable to retrieve the correlation energy and hence falls out of the chemical accuracy. On the other hand, substantial improvement is observed with the incorporation of ASC as it remains well within the chemical accuracy even with larger Ω values for all these cases. Particularly for stretched geometries, in the case of H_4 and H_6 in Fig. 4 ((D), (E)), the CNOT (parameter) count for SPQE to enter the $0.5 mE_h$ accuracy zone (pink shaded area) is ~ 3700 (15) with $\Omega=0.02$ and 80×10^3 (130) with $\Omega=0.02$, respectively. On the other hand AD(SPQE)-ASC enters the accuracy zone (gray region) around $\Omega = 0.05$ and 0.06 with the CNOT (parameter) count ~ 750 (10) and 28×10^3 (75) respectively, showing a drastic reduction in the associated circuit resources. Similar trend is ob-

served for H_2O as well as demonstrated in Figs. 3(C, F) and 4(C, F).

As discussed earlier in section IIB, the number of residual element evaluations are same for SPQE and AD(SPQE)-ASC as the *principal-to-auxiliary mapping* (Eq. (16)) can be in principle extracted directly from the last step of SPQE. However, for dynamic algorithms other than SPQE, the number of additional residual elements is $\dim\{APS\} = N_A$ at worst. The evaluation of ASC for scheme-II requires some extra diagonal matrix elements (see last term of Eq. (20)) which is significantly less than the cost of SPQE. Some quantitative discussions regarding the measurement cost is discussed in Appendix D.

IV. CONCLUSION AND FUTURE OUTLOOK

In this article, we introduce a general theoretical framework having structure like AD(x)-ASC (“x” denotes the method for preparing the core), designed to deliver highly accurate energy calculations while significantly reducing the quantum resource requirements to implement the dynamic ansatz. In this particular work, we build upon SPQE algorithm, which employs an “evolve-and-measure” strategy for dynamic ansatz construction via alternate macro and micro-iteration cycles. We argue that SPQE naturally induces adiabatic approximation, resulting in bipartite decoupling of the operator pool. The core (involving PPS) of the ansatz is formed via SPQE where only minimal number of *principal* operators are chosen through repeated quantum measurements. The remaining operators form the *auxiliary* operator subspace, with parameters that can be predicted from the optimized *principal* parameters using a mathematical relationship established in this work. Further, the contributions of *auxiliary* operators are incorporated into the energy function via a set of non-iterative corrections referred to as ASC. Thus both parts of the ansatz are flexible, while they sum up to a predefined set of operator pool with fixed number of operators. The hallmark of this entire AD(SPQE)-ASC protocol is that ASC does not require any additional circuit resources as the circuit depth of the ansatz is explicitly governed by SPQE. Moreover, we demonstrated that AD(SPQE)-ASC does not require any extra residual elements evaluations.

All of our numerical studies indicate that AD(SPQE)-ASC can substantially retrieve the electronic correlation energy in the strongly correlated regime of the PES, even with only SD operators in the core ansatz. It shows astounding performance specially with higher values of the operator selection threshold where the core SPQE ansatz is not adequately accurate itself, but extremely compact. We have also analytically and numerically substantiated that for achieving a particular order of accuracy, AD(SPQE)-ASC requires significantly less number of CNOT gates and number of measurements as compared to SPQE. Such exceptionally accurate performance

of AD(SPQE)-ASC with lower utilization of quantum resource requirements indicate the significance of the suite of non-iterative corrections. Even though we considered a projective formalism here, AD(x)-ASC is a general framework that can be coupled with other dynamic ansatz protocols like ADAPT-VQE²¹ or COMPASS²³ for better accuracy and resource efficiency which will be pursued as separate studies.

V. ACKNOWLEDGMENTS

RM acknowledges the financial support from Industrial Research and Consultancy Centre (IRCC), IIT Bombay and Science and Engineering Research Board (SERB), Government of India (Grant Number: MTR/2023/001306). CP and SH acknowledges University Grants Commission (UGC) Council of Scientific and Industrial Research (CSIR) for their respective research fellowships. DM acknowledges Prime Minister’s Research Fellowship (PMRF) for his research fellowship.

AUTHOR DECLARATIONS

Conflict of Interest:

The authors have no conflict of interest to disclose.

DATA AVAILABILITY

The data is available upon reasonable request to the corresponding author.

Appendix A: Discussion on adiabatic approximation and the determination of *auxiliary* parameters from the SPQE-selected *principal* parameters

In this appendix, we discuss the adiabatic approximation and slaving principle for determination of the *auxiliary* parameters from the *principal* ones selected by SPQE. With the decoupling of the parameter space, in general we can write down the parameter variation (or update) equation for both class of parameters

$$\Delta\theta_\xi = \frac{r_\xi}{D_\xi}; \quad \xi \in APS \text{ or } PPS \quad (A1)$$

where, ξ is a composite hole-particle indices that can belong to *principal* or *auxiliary* subsets. Since the residuals r_ξ are inherently nonlinear, we can reorder the terms

$$\Delta\theta_\xi = \Lambda_\xi\theta_\xi + M_\xi(\boldsymbol{\theta}_P, \boldsymbol{\theta}_A) \quad (A2)$$

where, Λ_ξ is the coefficient of the linear diagonal term

$$\Lambda_\xi = \frac{1}{D_\xi} \langle \Phi_\xi | [\hat{H}, \hat{\kappa}_\xi] | \Phi_0 \rangle \quad (A3)$$

and M_ξ contains all the nonlinear and linear off-diagonal terms

$$M_\xi(\boldsymbol{\theta}_P, \boldsymbol{\theta}_A) = \frac{1}{D_\xi} \langle \Phi_\xi | \hat{H} + \sum_{\nu \neq \xi} \theta_\nu [\hat{H}, \hat{\kappa}_\nu] + \sum_\nu \sum_\mu \theta_\nu \theta_\mu \left[[\hat{H}, \hat{\kappa}_\nu], \hat{\kappa}_\mu \right] + \dots | \Phi_0 \rangle \quad (\text{A4})$$

Due to the relatively slower convergence of the *principal* parameters, the variation of the *auxiliary* parameters can be neglected in the characteristic convergence timescale of the *principal* parameters. This is known as the *adiabatic approximation*^{51,53,54}. Due to this, we can set *auxiliary* variation $\Delta\theta_{A_\alpha} = 0$ in the update equation Eq. (A2)

$$0 = \Lambda_{A_\alpha} \theta_{A_\alpha} + M_{A_\alpha}(\boldsymbol{\theta}_P, \boldsymbol{\theta}_A) \quad (\text{A5})$$

With this we can re-order Eq. (A5) for the adiabatic solution of the *auxiliary* parameters

$$\theta_{A_\alpha} = -\frac{M_{A_\alpha}(\boldsymbol{\theta}_P, \boldsymbol{\theta}_A)}{\Lambda_{A_\alpha}} \quad (\text{A6})$$

Further, we can invoke the relative magnitude condition (Eq. (10)) to express the *auxiliary* parameters as a function of *principal* parameters only

$$\theta_{A_\alpha} = -\frac{M_{A_\alpha}(\boldsymbol{\theta}_P, \boldsymbol{\theta}_A)}{\Lambda_{A_\alpha}} \xrightarrow{|\theta_A| \ll |\theta_P|} \approx -\frac{M_{A_\alpha}(\boldsymbol{\theta}_P)}{\Lambda_{A_\alpha}} \quad (\text{A7})$$

From Eq. (A4) one can write $M_{A_\alpha}(\boldsymbol{\theta}_P)$ explicitly as

$$M_{A_\alpha}(\boldsymbol{\theta}_P) \approx \frac{1}{D_{A_\alpha}} \langle \Phi_{A_\alpha} | \hat{H} + \sum_{P_I} \theta_{P_I} [\hat{H}, \hat{\kappa}_{P_I}] + \sum_{P_I} \sum_{P_J} \theta_{P_I} \theta_{P_J} \left[[\hat{H}, \hat{\kappa}_{P_I}], \hat{\kappa}_{P_J} \right] + \dots | \Phi_0 \rangle \quad (\text{A8})$$

$$= \frac{\langle \Phi_{A_\alpha} | \hat{U}_P^\dagger(\boldsymbol{\theta}_P) \hat{H} \hat{U}_P(\boldsymbol{\theta}_P) | \Phi_0 \rangle}{D_{A_\alpha}}$$

Using the expression obtained in Eq. (A8), Eq. (A7) can be compactly written as-

$$\theta_{A_\alpha} = -\frac{\langle \Phi_{A_\alpha} | \hat{U}_P^\dagger(\boldsymbol{\theta}_P) \hat{H} \hat{U}_P(\boldsymbol{\theta}_P) | \Phi_0 \rangle}{\langle \Phi_{A_\alpha} | [\hat{H}, \hat{\kappa}_{A_\alpha}] | \Phi_0 \rangle} \quad (\text{A9})$$

$$= \frac{\langle \Phi_{A_\alpha} | \hat{U}_P^\dagger(\boldsymbol{\theta}_P) \hat{H} \hat{U}_P(\boldsymbol{\theta}_P) | \Phi_0 \rangle}{D_{A_\alpha}}$$

where, $\langle \Phi_{A_\alpha} | [\hat{H}, \hat{\kappa}_{A_\alpha}] | \Phi_0 \rangle \approx -D_{A_\alpha}$ under leading order approximation (see Appendix (B)).

Appendix B: First Order Approximation of Commutator Expectation Values

In this section, we provide a mathematical details of the approximation of the denominator for *auxiliary* solution Eq. (A9). The commutator $\langle \Phi_\mu | [\hat{H}, \hat{\kappa}_\nu] | \Phi_0 \rangle$ can

be approximated by expanding the Hamiltonian into a zeroth-order one-body Fock operator and a first-order two-body operator, $\hat{H} = \hat{F}^{(0)} + \hat{V}^{(1)}$. Retaining only the zeroth-order term we get

$$\langle \Phi_\mu | [\hat{H}, \hat{\kappa}_\nu] | \Phi_0 \rangle \Rightarrow \langle \Phi_\mu | [\hat{F}^{(0)}, \hat{\kappa}_\nu] | \Phi_0 \rangle \approx -D_\mu \delta_{\mu\nu} \quad (\text{B1})$$

Appendix C: Derivation of the low depth energy determining equation with non-iterative corrections

Here, we analytically establish the energy expression for scheme-I (Eq. (19)) and scheme-II (Eq. (20)) for a shallow-depth inclusion of the *auxiliary* parameters into the energy functional. With the *principal-auxiliary bipartite* operator (Eq. (11)), the energy term can be expressed by

$$E(\boldsymbol{\theta}) = \langle \Phi_0 | \hat{U}_{pab}^\dagger(\boldsymbol{\theta}) H \hat{U}_{pab}(\boldsymbol{\theta}) | \Phi_0 \rangle \quad (\text{C1})$$

Term 1 and *Term 2* in Eq. (17) can be further expanded as follows:

Term 1

$$\begin{aligned} & \theta_{A_\alpha} \langle \Phi_0 | [\bar{H}_P, \hat{\kappa}_{A_\alpha}] | \Phi_0 \rangle \\ &= \theta_{A_\alpha} \langle \Phi_0 | \bar{H}_P \hat{\kappa}_{A_\alpha} | \Phi_0 \rangle - \langle \Phi_0 | \hat{\kappa}_{A_\alpha} \bar{H}_P | \Phi_0 \rangle \\ &= \theta_{A_\alpha} \langle \Phi_0 | \bar{H}_P | \Phi_{A_\alpha} \rangle + \langle \Phi_{A_\alpha} | \bar{H}_P | \Phi_0 \rangle \quad (\text{C2}) \\ &= 2\theta_{A_\alpha} \langle \Phi_{A_\alpha} | \hat{U}_P^\dagger \hat{H} \hat{U}_P | \Phi_0 \rangle \\ &= 2\theta_{A_\alpha}^2 D_{A_\alpha} \end{aligned}$$

where, at the last step, we have used Eq. (16) to replace the operator expectation value with adiabatically obtained *auxiliary* parameters.

Term 2

Since *Term 2* is a nonlinear term, for its evaluation, we first approximate the BCH expansion for \bar{H}_P up to zeroth order, which is just the bare Hamiltonian

$$\langle \Phi_0 | \left[[\bar{H}_P, \hat{\kappa}_{A_\alpha}], \hat{\kappa}_{A_\beta} \right] | \Phi_0 \rangle \approx \langle \Phi_0 | \left[[\hat{H}, \hat{\kappa}_{A_\alpha}], \hat{\kappa}_{A_\beta} \right] | \Phi_0 \rangle \quad (\text{C3})$$

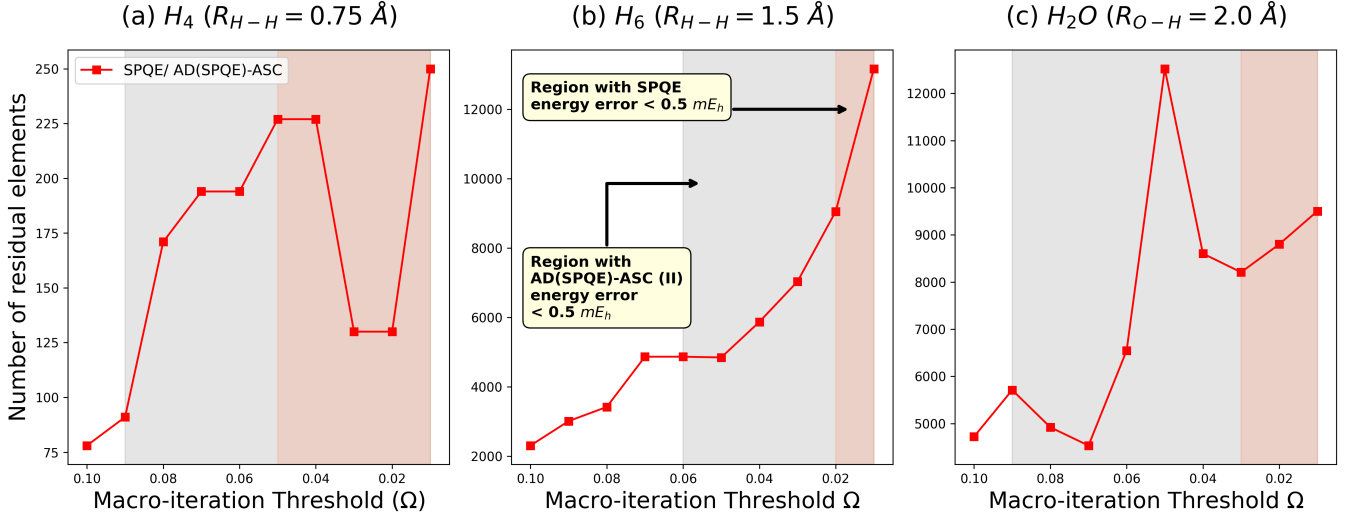


FIG. 5. Number of residue element evaluations for SPQE and AD(SPQE)-ASC (with SDTQ pool) with different macro-iteration threshold (Ω). Note that, the number of residue elements for both the methods are same for a particular value of Ω . However, for attaining similar order of accuracy, AD(SPQE)-ASC (II) requires less number of residue elements than SPQE as represented by different shaded regions (see the subplot corresponding to column (b) for the details of the color coding).

For scheme-I, we can approximate the Hamiltonian to the zeroth order fock operator only for a simpler expression

$$\begin{aligned}
& \frac{1}{2} \theta_{A_\alpha} \theta_{A_\beta} \langle \Phi_0 | [[\bar{H}_P, \hat{\kappa}_{A_\alpha}], \hat{\kappa}_{A_\beta}] | \Phi_0 \rangle \\
& \approx \frac{1}{2} \theta_{A_\alpha} \theta_{A_\beta} \langle \Phi_0 | [[\hat{H}, \hat{\kappa}_{A_\alpha}], \hat{\kappa}_{A_\beta}] | \Phi_0 \rangle \\
& \approx \frac{1}{2} \theta_{A_\alpha} \theta_{A_\beta} \left(\langle \Phi_0 | [\hat{F}^{(0)}, \hat{\kappa}_{A_\alpha}] \hat{\kappa}_{A_\beta} | \Phi_0 \rangle - \right. \\
& \quad \left. \langle \Phi_0 | \hat{\kappa}_{A_\beta} [\hat{F}^{(0)}, \hat{\kappa}_{A_\alpha}] | \Phi_0 \rangle \right) \\
& = \frac{1}{2} \theta_{A_\alpha} \theta_{A_\beta} \left(\langle \Phi_0 | [\hat{F}^{(0)}, \hat{\kappa}_{A_\alpha}] | \Phi_{A_\beta} \rangle + \right. \\
& \quad \left. \langle \Phi_{A_\beta} | [\hat{F}^{(0)}, \hat{\kappa}_{A_\alpha}] | \Phi_0 \rangle \right) \\
& = \theta_{A_\alpha} \theta_{A_\beta} \langle \Phi_{A_\beta} | [\hat{F}^{(0)}, \hat{\kappa}_{A_\alpha}] | \Phi_0 \rangle \\
& \approx -\theta_{A_\alpha} \theta_{A_\beta} D_{A_\beta} \delta_{A_\alpha A_\beta}
\end{aligned} \tag{C4}$$

where, at the last step we have used the expression in Eq. (B1). Plugging the final forms of *Term 1* (Eq. (C2)) and *Term 2* (Eq. (C4)) in Eq. (17) we get the scheme-I energy expression Eq. (19). In Eq. (C4) the contributions from the off-diagonal terms are zero due to the presence of the delta function. Even in the general case, the contributions from the off-diagonal terms are negligible such that Eq. (C3) can be assumed to contain only diagonal terms which leads to the following expression

$$\langle \Phi_0 | [[\bar{H}_P, \hat{\kappa}_{A_\alpha}], \hat{\kappa}_{A_\beta}] | \Phi_0 \rangle \approx \langle \Phi_0 | [[\hat{H}, \hat{\kappa}_{A_\alpha}], \hat{\kappa}_{A_\beta}] | \Phi_0 \rangle \tag{C5}$$

Plugging this along with the expression obtained in Eq. (C2) into energy expression Eq. (17) results in the scheme-II energy equation Eq. (20) which is more accurate than scheme-I as discussed in section III.

Appendix D: Measurement overhead for auxiliary subspace correction terms

The number of measurements in SPQE for all the micro-iterations is of the order of¹³

$$M_{SPQE} \leq N_{res} \times 3N_P \frac{(\sum_l h_l)^2}{\epsilon^2} \tag{D1}$$

while, the measurement overhead required to converge SPQE macro-iterations with threshold Ω is $\sim (\Delta t \Omega)^{-2}$. Here, N_{res} is the total number of residual vectors evaluated during all of the micro-iteration optimization, h_l is the coefficient of l -th Pauli string in the Jordan-Wigner mapped Hamiltonian and ϵ is the desired precision in measurement based energy estimation. Since the mapped *auxiliary* parameters via Eq. (16) can directly be obtained from SPQE-excluded residuals, scheme-I does not require any additional measurements.

The additional measurement for ASC in scheme-II due to the third term of Eq. (20) is

$$M_{II} \leq N_A \frac{(\sum_l h_l)^2}{\epsilon^2} \tag{D2}$$

This additional measurement cost M_{II} stems from $\langle \Phi_0 | * | \Phi_0 \rangle$ type of measurements in Eq. (20). Thus the total measurement cost of AD(SPQE)-ASC (II) becomes

$$M_{AD(SPQE)-ASC} = M_{SPQE} + M_{II} \tag{D3}$$

For scheme-II, the additional cost for ASC (M_{II}) is in general less than that of SPQE (M_{SPQE}) as N_A is usually less than $(N_{res} \times 3N_P)$ for all practical scenarios. Note that, both the schemes of AD(SPQE)-ASC do not

require any extra residual elements to be evaluated in addition to that of SPQE. In Fig. 5 we have shown the number of residue element evaluations for different Ω values. Note that the curve enters the gray region with much less number of residue element count which represents that for attaining similar order of accuracy (in this case $< 0.5 mE_h$), AD(SPQE)-ASC (II) requires much less number of residue elements (and measurements) to be evaluated than standard SPQE.

REFERENCES:

- ¹S. R. White, "Density matrix formulation for quantum renormalization groups," *Physical review letters* **69**, 2863 (1992).
- ²B. Huron, J. Malrieu, and P. Rancurel, "Iterative perturbation calculations of ground and excited state energies from multiconfigurational zeroth-order wavefunctions," *The Journal of Chemical Physics* **58**, 5745–5759 (1973).
- ³R. J. Buenker and S. D. Peyerimhoff, "Individualized configuration selection in ci calculations with subsequent energy extrapolation," *Theoretica chimica acta* **35**, 33–58 (1974).
- ⁴J. Čížek, "On the correlation problem in atomic and molecular systems. calculation of wavefunction components in urself-type expansion using quantum-field theoretical methods," *J. Chem. Phys.* **45**, 4256–4266 (1966).
- ⁵J. Čížek, "On the use of the cluster expansion and the technique of diagrams in calculations of correlation effects in atoms and molecules," *Adv. Chem. Phys.* **14**, 35–89 (1969).
- ⁶J. Čížek and J. Paldus, "Correlation problems in atomic and molecular systems iii. rederivation of the coupled-pair many-electron theory using the traditional quantum chemical methods," *Int. J. Quantum Chem.* **5**, 359–379 (1971).
- ⁷R. J. Bartlett and M. Musiał, "Coupled-cluster theory in quantum chemistry," *Reviews of Modern Physics* **79**, 291 (2007).
- ⁸T. D. Crawford and H. F. Schaefer, "An introduction to coupled cluster theory for computational chemists," *Reviews in computational chemistry* **14**, 33–136 (2000).
- ⁹D. S. Abrams and S. Lloyd, "Simulation of many-body fermi systems on a universal quantum computer," *Physical Review Letters* **79**, 2586 (1997).
- ¹⁰D. S. Abrams and S. Lloyd, "Quantum algorithm providing exponential speed increase for finding eigenvalues and eigenvectors," *Physical Review Letters* **83**, 5162 (1999).
- ¹¹J. Preskill, "Quantum computing in the nisq era and beyond," *Quantum* **2**, 79 (2018).
- ¹²A. Peruzzo, J. McClean, P. Shadbolt, M.-H. Yung, X.-Q. Zhou, P. J. Love, A. Aspuru-Guzik, and J. L. O'Brien, "A variational eigenvalue solver on a photonic quantum processor," *Nature communications* **5**, 4213 (2014).
- ¹³N. H. Stair and F. A. Evangelista, "Simulating many-body systems with a projective quantum eigensolver," *PRX Quantum* **2**, 030301 (2021).
- ¹⁴K. Temme, S. Bravyi, and J. M. Gambetta, "Error mitigation for short-depth quantum circuits," *Physical review letters* **119**, 180509 (2017).
- ¹⁵C. Song, J. Cui, H. Wang, J. Hao, H. Feng, and Y. Li, "Quantum computation with universal error mitigation on a superconducting quantum processor," *Science advances* **5**, eaaw5686 (2019).
- ¹⁶S. Zhang, Y. Lu, K. Zhang, W. Chen, Y. Li, J.-N. Zhang, and K. Kim, "Error-mitigated quantum gates exceeding physical fidelities in a trapped-ion system," *Nature communications* **11**, 587 (2020).
- ¹⁷B. Koczor, "Exponential error suppression for near-term quantum devices," *Physical Review X* **11**, 031057 (2021).
- ¹⁸W. J. Huggins, S. McArdle, T. E. O'Brien, J. Lee, N. C. Rubin, S. Boixo, K. B. Whaley, R. Babbush, and J. R. McClean, "Virtual distillation for quantum error mitigation," *Physical Review X* **11**, 041036 (2021).
- ¹⁹Z. Cai, R. Babbush, S. C. Benjamin, S. Endo, W. J. Huggins, Y. Li, J. R. McClean, and T. E. O'Brien, "Quantum error mitigation," *Reviews of Modern Physics* **95**, 045005 (2023).
- ²⁰R. Takagi, S. Endo, S. Minagawa, and M. Gu, "Fundamental limits of quantum error mitigation," *npj Quantum Information* **8**, 114 (2022).
- ²¹H. R. Grimsley, S. E. Economou, E. Barnes, and N. J. Mayhall, "An adaptive variational algorithm for exact molecular simulations on a quantum computer," *Nature communications* **10**, 3007 (2019).
- ²²A. Delgado, J. M. Arrazola, S. Jahangiri, Z. Niu, J. Izaac, C. Roberts, and N. Killoran, "Variational quantum algorithm for molecular geometry optimization," *Physical Review A* **104**, 052402 (2021).
- ²³D. Mondal, D. Halder, S. Halder, and R. Maitra, "Development of a compact Ansatz via operator commutativity screening: Digital quantum simulation of molecular systems," *The Journal of Chemical Physics* **159**, 014105 (2023).
- ²⁴C. Feniou, M. Hassan, D. Traoré, E. Giner, Y. Maday, and J.-P. Piquemal, "Overlap-adapt-vqe: practical quantum chemistry on quantum computers via overlap-guided compact ansätze," *Communications Physics* **6**, 192 (2023).
- ²⁵L. Zhao, J. Goings, K. Shin, W. Kyoung, J. I. Fuks, J.-K. Kevin Rhee, Y. M. Rhee, K. Wright, J. Nguyen, J. Kim, *et al.*, "Orbital-optimized pair-correlated electron simulations on trapped-ion quantum computers," *npj Quantum Information* **9**, 60 (2023).
- ²⁶H. L. Tang, V. Shkolnikov, G. S. Barron, H. R. Grimsley, N. J. Mayhall, E. Barnes, and S. E. Economou, "qubit-adapt-vqe: An adaptive algorithm for constructing hardware-efficient ansätze on a quantum processor," *PRX Quantum* **2**, 020310 (2021).
- ²⁷M. Ostaszewski, E. Grant, and M. Benedetti, "Structure optimization for parameterized quantum circuits," *Quantum* **5**, 391 (2021).
- ²⁸N. V. Tkachenko, J. Sud, Y. Zhang, S. Tretiak, P. M. Anisimov, A. T. Arrasmith, P. J. Coles, L. Cincio, and P. A. Dub, "Correlation-informed permutation of qubits for reducing ansatz depth in the variational quantum eigensolver," *PRX Quantum* **2**, 020337 (2021).
- ²⁹F. Zhang, N. Gomes, Y. Yao, P. P. Orth, and T. Iadecola, "Adaptive variational quantum eigensolvers for highly excited states," *Physical Review B* **104**, 075159 (2021).
- ³⁰S. Sim, J. Romero, J. F. Gonthier, and A. A. Kunita, "Adaptive pruning-based optimization of parameterized quantum circuits," *Quantum Science and Technology* **6**, 025019 (2021).
- ³¹D. Halder, V. S. Prasanna, and R. Maitra, "Dual exponential coupled cluster theory: Unitary adaptation, implementation in the variational quantum eigensolver framework and pilot applications," *The Journal of Chemical Physics* **157**, 174117 (2022).
- ³²D. Halder, S. Halder, D. Mondal, C. Patra, A. Chakraborty, and R. Maitra, "Corrections beyond coupled cluster singles and doubles through selected generalized rank-two operators: digital quantum simulation of strongly correlated systems," *Journal of Chemical Sciences* **135**, 41 (2023).
- ³³S. Halder, C. Patra, D. Mondal, and R. Maitra, "Machine learning aided dimensionality reduction toward a resource efficient projective quantum eigensolver: Formal development and pilot applications," *The Journal of Chemical Physics* **158** (2023).
- ³⁴S. Liu, S.-X. Zhang, S.-K. Jian, and H. Yao, "Training variational quantum algorithms with random gate activation," *Physical Review Research* **5**, L032040 (2023).
- ³⁵S. Halder, A. Dey, C. Shrikhande, and R. Maitra, "Machine learning assisted construction of a shallow depth dynamic ansatz for noisy quantum hardware," *Chem. Sci.* **15**, 3279–3289 (2024).
- ³⁶S. G. Mehendale, B. Peng, N. Govind, and Y. Alexeev, "Exploring parameter redundancy in the unitary coupled-cluster ansatz for hybrid variational quantum computing," *The Journal of Physical Chemistry A* (2023).

- ³⁷I. G. Ryabinkin, T.-C. Yen, S. N. Genin, and A. F. Izmaylov, "Qubit coupled cluster method: a systematic approach to quantum chemistry on a quantum computer," *Journal of chemical theory and computation* **14**, 6317–6326 (2018).
- ³⁸I. G. Ryabinkin, R. A. Lang, S. N. Genin, and A. F. Izmaylov, "Iterative qubit coupled cluster approach with efficient screening of generators," *Journal of chemical theory and computation* **16**, 1055–1063 (2020).
- ³⁹Y. S. Yordanov, D. R. Arvidsson-Shukur, and C. H. Barnes, "Efficient quantum circuits for quantum computational chemistry," *Physical Review A* **102**, 062612 (2020).
- ⁴⁰I. Magoulas and F. A. Evangelista, "Cnot-efficient circuits for arbitrary rank many-body fermionic and qubit excitations," *Journal of Chemical Theory and Computation* **19**, 822–836 (2023).
- ⁴¹K. Kowalski, "Dimensionality reduction of the many-body problem using coupled-cluster subsystem flow equations: Classical and quantum computing perspective," *Physical Review A* **104**, 032804 (2021).
- ⁴²K. Kowalski and N. P. Bauman, "Quantum flow algorithms for simulating many-body systems on quantum computers," *Physical Review Letters* **131**, 200601 (2023).
- ⁴³R. Huang, C. Li, and F. A. Evangelista, "Leveraging small-scale quantum computers with unitarily downfolded hamiltonians," *PRX Quantum* **4**, 020313 (2023).
- ⁴⁴N. P. Bauman, E. J. Bylaska, S. Krishnamoorthy, G. H. Low, N. Wiebe, C. E. Granade, M. Roetteler, M. Troyer, and K. Kowalski, "Downfolding of many-body hamiltonians using active-space models: Extension of the sub-system embedding sub-algebras approach to unitary coupled cluster formalisms," *The Journal of Chemical Physics* **151**, 014107 (2019).
- ⁴⁵M. Metcalf, N. P. Bauman, K. Kowalski, and W. A. De Jong, "Resource-efficient chemistry on quantum computers with the variational quantum eigensolver and the double unitary coupled-cluster approach," *Journal of chemical theory and computation* **16**, 6165–6175 (2020).
- ⁴⁶P. Piecuch and L. Adamowicz, "Solving the single-reference coupled-cluster equations involving highly excited clusters in quasidegenerate situations," *The Journal of chemical physics* **100**, 5857–5869 (1994).
- ⁴⁷K. Kowalski and P. Piecuch, "The method of moments of coupled-cluster equations and the renormalized CCSD [T], CCSD (T), CCSD (TQ), and CCSDT (Q) approaches," *The Journal of Chemical Physics* **113**, 18–35 (2000).
- ⁴⁸I. Magoulas and F. A. Evangelista, "Unitary coupled cluster: Seizing the quantum moment," *The Journal of Physical Chemistry A* **127**, 6567–6576 (2023).
- ⁴⁹B. Peng and K. Kowalski, "Mapping renormalized coupled cluster methods to quantum computers through a compact unitary representation of nonunitary operators," *Physical Review Research* **4**, 043172 (2022).
- ⁵⁰D. Claudino, B. Peng, N. P. Bauman, K. Kowalski, and T. S. Humble, "Improving the accuracy and efficiency of quantum connected moments expansions," *Quantum Science and Technology* **6**, 034012 (2021).
- ⁵¹C. Patra, S. Halder, and R. Maitra, "Projective quantum eigensolver via adiabatically decoupled subsystem evolution: A resource efficient approach to molecular energetics in noisy quantum computers," *The Journal of Chemical Physics* **160** (2024).
- ⁵²D. Halder, D. Mondal, and R. Maitra, "Noise-independent route toward the genesis of a compact ansatz for molecular energetics: A dynamic approach," *The Journal of Chemical Physics* **160** (2024).
- ⁵³C. Patra, V. Agarawal, D. Halder, A. Chakraborty, D. Mondal, S. Halder, and R. Maitra, "A synergistic approach towards optimization of coupled cluster amplitudes by exploiting dynamical hierarchy," *ChemPhysChem* **24**, e202200633 (2023).
- ⁵⁴V. Agarawal, C. Patra, and R. Maitra, "An approximate coupled cluster theory via nonlinear dynamics and synergetics: The adiabatic decoupling conditions," *The Journal of Chemical Physics* **155**, 124115 (2021).
- ⁵⁵S. Halder, C. Shrikhande, and R. Maitra, "Development of zero-noise extrapolated projective quantum algorithm for accurate evaluation of molecular energetics in noisy quantum devices," *The Journal of Chemical Physics* **159** (2023).
- ⁵⁶V. Agarawal, S. Roy, A. Chakraborty, and R. Maitra, "Accelerating coupled cluster calculations with nonlinear dynamics and supervised machine learning," *The Journal of Chemical Physics* **154**, 044110 (2021).
- ⁵⁷V. Agarawal, S. Roy, K. K. Shrawankar, M. Ghogale, S. Bharathi, A. Yadav, and R. Maitra, "A hybrid coupled cluster-machine learning algorithm: Development of various regression models and benchmark applications," *The Journal of Chemical Physics* **156**, 014109 (2022).
- ⁵⁸F. A. Evangelista, G. K.-L. Chan, and G. E. Scuseria, "Exact parameterization of fermionic wave functions via unitary coupled cluster theory," *The Journal of chemical physics* **151**, 244112 (2019).
- ⁵⁹S. H. Strogatz, *Nonlinear dynamics and chaos: with applications to physics, biology, chemistry, and engineering* (CRC press, 2018).
- ⁶⁰H. Haken, "Nonlinear equations. the slaving principle," in *Advanced Synergetics* (Springer, 1983) pp. 187–221.
- ⁶¹A. Wunderlin and H. Haken, "Generalized ginzburg-landau equations, slaving principle and center manifold theorem," *Zeitschrift für Physik B Condensed Matter* **44**, 135–141 (1981).
- ⁶²P. Piecuch and K. Kowalski, "In search of the relationship between multiple solutions characterizing coupled-cluster theories," in *Computational chemistry: reviews of current trends* (World Scientific, 2000) pp. 1–104.
- ⁶³K. Kowalski and P. Piecuch*, "New classes of non-iterative energy corrections to multi-reference coupled-cluster energies," *Molecular Physics* **102**, 2425–2449 (2004).
- ⁶⁴J. Pittner and P. Piecuch, "Method of moments for the continuous transition between the brillouin-wigner-type and rayleigh-schrödinger-type multireference coupled cluster theories," *Molecular Physics* **107**, 1209–1221 (2009).
- ⁶⁵N. H. Stair and F. A. Evangelista, "Qforte: An efficient state-vector emulator and quantum algorithms library for molecular electronic structure," *Journal of Chemical Theory and Computation* **18**, 1555–1568 (2022).
- ⁶⁶A. Javadi-Abhari, M. Treinish, K. Krsulich, C. J. Wood, J. Lishman, J. Gacon, S. Martiel, P. D. Nation, L. S. Bishop, A. W. Cross, B. R. Johnson, and J. M. Gambetta, "Quantum computing with Qiskit," (2024), arXiv:2405.08810 [quant-ph].
- ⁶⁷Q. Sun, T. C. Berkelbach, N. S. Blunt, G. H. Booth, S. Guo, Z. Li, J. Liu, J. D. McClain, E. R. Sayfutyarova, S. Sharma, *et al.*, "Pyscf: the python-based simulations of chemistry framework," *Wiley Interdisciplinary Reviews: Computational Molecular Science* **8**, e1340 (2018).
- ⁶⁸D. G. Smith, L. A. Burns, A. C. Simmonett, R. M. Parrish, M. C. Schieber, R. Galvelis, P. Kraus, H. Kruse, R. Di Remigio, A. Alenaizan, *et al.*, "Psi4 1.4: Open-source software for high-throughput quantum chemistry," *The Journal of chemical physics* **152** (2020).
- ⁶⁹P. Jordan and E. P. Wigner, *Über das paulische äquivalenzverbot* (Springer, 1993).